






Delaying two-photon Fock states in hot cesium vapor using single photons generated on demand from a semiconductor quantum dot

H. Vural ¹, S. Seyfferle ¹, I. Gerhardt ², M. Jetter ¹, S. L. Portalupi,¹ and P. Michler ^{1,*}

¹*Institut für Halbleiteroptik und Funktionelle Grenzflächen, Center for Integrated Quantum Science and Technology (IQST) and SCoPE, University of Stuttgart, Allmandring 3, 70569 Stuttgart, Germany*

²*3. Physikalisches Institut and Center for Integrated Quantum Science and Technology, University of Stuttgart, Pfaffenwaldring 57, D-70569 Stuttgart, Germany*



(Received 7 October 2020; revised 16 April 2021; accepted 19 April 2021; published 5 May 2021)

Single photons from solid-state quantum emitters are playing a crucial role in the development of photonic quantum technologies and, by extension, higher order states, such as N -photon Fock states, allow for applications, e.g., in quantum-enhanced sensing. To verify the applicability of these states in future quantum technological implementations involving photon-atom interactions (i.e., storage of a quantum state in alkali vapor and photon delay) we utilize in the present study the dispersion of a hot cesium vapor at the D_1 line to realize a temporal delay for two-photon Fock states as a result of the slow-light effect. Single photons are generated on demand from an InGaAs quantum dot, while their quantum interference at a beam splitter is used to generate a two-photon Fock state. We verify the successful propagation and the preservation of the two-photon Fock states after the interaction with the slow-light medium, while a significant temporal delay (five times the initial photon length) is achieved with a high vapor transmission of 90%.

DOI: [10.1103/PhysRevB.103.195304](https://doi.org/10.1103/PhysRevB.103.195304)

I. INTRODUCTION

Self-assembled semiconductor quantum dots (QDs) are one of the appealing platforms for the realization of optical quantum technologies [1]. Under resonant π -pulse excitation QDs are promising on-demand emitters of coherent, indistinguishable single [2] and entangled photons [3,4]. The ultrahigh rates of single photons achieved by integration of QDs in photonic cavity structures pushed the frontier of this photonic technology to a level competitive with computer simulations in special tasks like boson sampling [5].

Moreover, multiphoton entangled states, mainly in the form of two-photon states, play a major role for quantum technology applications such as quantum enhanced metrology [6–8], quantum key distribution [9], as well as for the implementation of quantum repeaters [10] and even in fields such as two-photon microscopy [11]. Additionally, two-photon Fock states $|2\rangle$ in a superposition of two (spatial) modes, referred to as N00N states ($N = 2$), are promising candidates for interferometry with superresolution and sensitivity beating the standard quantum limit [6–8,12].

Theoretical proposals for efficient two-photon Fock-state generation from semiconductor QDs have been put forth involving cavity-enhanced recombination [13–15]; however, the realization of actual Fock states directly emitted by a single solid-state source is still elusive. Two-photon states have been identified experimentally in the superradiant emission of two quantum dots coupled to the same waveguide mode [16], which is a structure hard to realize. Additionally, scaling is

an issue due to decoherence in multisource applications that are more critical than for single-source ones [17–19]. Using a single QD two-level system experimental demonstrations have already been conducted observing multiphoton emission due to the systems reexcitation during a resonant 2π -pulse excitation [20,21]. However, two-photon states generated in this way are not pure and do not yet constitute actual Fock states since they do not share the same temporal mode, hence missing also their benefits.

Due to its primal importance storage of this quantum state of light has been studied in quantum memories recently. Two-photon Fock states from a parametric down-conversion source were delayed in an optical cavity [22], while two-photon N00N states, generated from photon-pair emission of cold atoms, were delayed by storage in a cold atomic ensemble as well [23]. High fractional delays of single photons have been realized in alkali vapor and the slow-light effect has been found to preserve photonic coherence [24]. The establishment of this robust storage medium also for multiphoton states is an important step, which is presented here for the case of two photons.

A practical means to prepare a two-photon N00N state is given by utilizing the Hong-Ou-Mandel (HOM) effect [25,26] for single and indistinguishable photons [8,12,23]. For this, π -pulse excitation of a QD is exploited, which leads to dominance of the one-photon Fock state $|1\rangle$ in the emission with vanishing multiphoton and vacuum contributions, thus being most suitable for the on-demand single-photon generation [20,21].

In this work, we take this approach to study the slow-light effect and the acquired delay in a hot cesium (Cs) vapor [28] for one-photon $|1\rangle$ and two-photon $|2\rangle$ Fock states. In

*p.michler@ihfg.uni-stuttgart.de

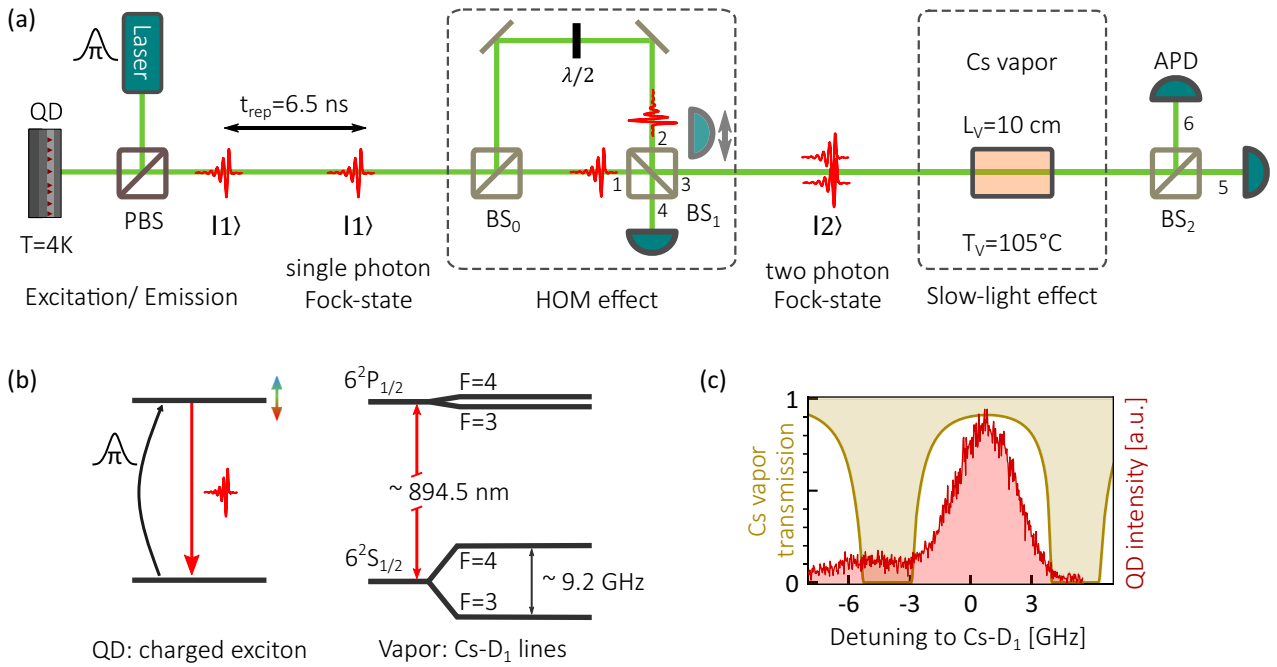


FIG. 1. Experimental scheme. (a) Sketch of the experimental setup: A quantum dot (QD) is excited by a resonant π pulse. The emitted single photons $|1\rangle$ are fed into an unbalanced Mach-Zehnder interferometer to generate probabilistically the two-photon Fock state $|2\rangle$ as a result of the Hong-Ou-Mandel (HOM) effect at the beam splitter (BS_1). One output port (3) can be linked to a slow-light medium [here cesium (Cs) vapor] of length $L_V = 10$ cm. After the beam splitter (BS_2) photon correlation and TCSPC are measured using single-photon counting modules (APD). (b) Illustration of the resonant pumping of the QD's charged exciton state and the following emission of a photon at the Cs- D_1 transition energy. (c) Simulation [27] of the vapor transmission at the operated temperature of $T_V = 105^\circ\text{C}$ alongside a measured emission spectrum of the QD.

doing so, we extend the present studies using QDs which were probed, so far, only single photons by delaying [24,29–31] or polarization-dependent routing [32] in a hot vapor, to the regime of the two-photon states.

A Cs vapor dispersive medium in combination with single QD photons recently proved highly effective for narrow bandwidth filtering by exploiting the Faraday effect [33]. Moreover, strong group velocity dispersion has been key to sensitive spectroscopic characterization of a QD's emission, particularly its spectral diffusion dynamics by mapping frequency domain to time domain [34]. As for two-photon Fock states, the effective combination with a slow-light medium can be useful to strengthen its interferometric phase estimation with superresolution and supersensitivity [6–8,12], since the steep dispersion in a vapor additionally enhances spectral phase sensitivity [35–37].

Experimental framework

To generate a stream of timed single photons, the charged exciton transition of a single InGaAs QD is excited via a short optical π pulse. The addressed state is identified via its power dependence and polarization characteristics. The wavelength of the QD transition is fine-tuned to the Cs- D_1 lines by the application of a uniaxial strain field [30,38] [Fig. 1(b)]. The resonant laser (3 ps pulse length, 6.5 ns repetition period) is suppressed by cross-polarized excitation and detection while the QD emission is filtered to direct the zero-phonon line into an unbalanced Mach-Zehnder interferometer [Fig. 1(a)].

This serves to realize probabilistically the HOM interference for successively emitted photons at the output beam splitter (BS_1). In fact, indistinguishable one-photon Fock states $|1\rangle$ entering at BS_1 from different ports will yield the state $\frac{1}{\sqrt{2}}(|2, 0\rangle - |0, 2\rangle)$ at the outputs, which is a path-entangled N00N state with both photons being in one port. Considering one output port allows to project out the $|2\rangle$ state and thus investigation of the two-photon Fock state.

HOM interference at a beam splitter is usually detected via the absence of coincidences (here, at ports 3 and 4), since both photons take the same path. The presence of emission line broadening, however, renders photons distinguishable, such that coincidences still do occur. The time-resolved coincidences then display beating [18,39] with a sharp dip in the correlation peak that depends on the broadening [see also Fig. 4(a) in the Appendix].

Successful two-photon interference can alternatively be detected by analyzing the photon statistics in one output arm, since the probability to find a photon pair is $\frac{1}{2}$ for indistinguishable inputs in contrast to $\frac{1}{4}$ for distinguishable photons. This can be measured through correlations after an additional beam splitter (BS_2). Here, a coincidence at the output ports (5 and 6) would testify a photon pair, as opposed to the arrival of single photons. The generation of two-photon Fock states and the resulting bunching of photons due to HOM interference at BS_1 is then signified by doubled coincidence counts. Furthermore, the beating in time-resolved coincidences at BS_1 implies an inverse temporal shape for the coincidence peak after BS_2 [see Fig. 4(b) in the Appendix]. With these two

characteristics, the important distinction between a pair of single photons in distinguishable modes and the actual $|2\rangle$ state can be made [16,40]. Moreover, the time-correlated detection of the $|2\rangle$ state is enabled, which will be propagated through a hot Cs vapor between the generation (BS_1) and analyzing (BS_2) beam splitters to study its interaction with the slow-light medium.

To investigate the vapor-induced delay, time-correlated single-photon counting (TCSPC) is performed that correlates the arrival time of photons at one APD to the excitation laser pulses. As for the $|2\rangle$ state, TCSPC is heralded by a coincidence detection (at ports 5 and 6). Only those cases are postselected, which allows one to measure the acquired delay for the photon pairs during the propagation through the slow-light medium.

Figure 1(c) shows the vapor transmission spectrum at the set temperature of $T_V = 105^\circ\text{C}$ for a cell length of $L_V = 10$ cm, which serves as the slow-light medium. At these conditions the speed of light is reduced by one order of magnitude between the Cs- D_1 hyperfine-split transitions. Still, the transmission window for the photons exceeds 90%. Figure 1(c) also compares the vapor transmission to the measured emission spectrum of the QD, which is shown while tuned to the center of the Cs- D_1 lines. The complex propagation of different spectral components in the vapor is reduced by tuning the QD to match the center of the transmission window [24,28]. The QD's spectrum is inhomogeneously broadened due to several decoherence mechanisms affecting the QD's two-level system [19,34,41–43]. These lead to spectral diffusion, which has been intensively studied for this particular QD in Ref. [34]. We note that the emission of the QD in consideration has an excellent single-photon purity, confirmed by photon correlation after a beam splitter [44] which yields $g^{(2)}(0) = 0.014 \pm 0.005$ and proves vanishing multiphoton contributions.

II. RESULTS

A. Generation of the two-photon Fock state

As a first step, we investigate the quantum interference at BS_1 , the benchmark measurement for the photon indistinguishability of the emitter. Figure 2(a) shows the photon-correlation histogram for the usual HOM measurement when detected at ports 3 and 4. Due to the possible paths consecutive photons can take in the HOM setup, a peak pattern arises where only the events within the central coincidence peak consist of the photons that entered the beam splitter simultaneously from different ports (1 and 2). When cross-polarized, noninterfering photons are investigated (orange curves), the coincidence peak amounts to half of the outermost peaks which relate to the Poissonian level. For the parallel-polarized case (blue curves), we find a strong reduction of coincidences with a dip within the peak. The coalescence reveals indistinguishability of successive photons [25,26], while the still present modulated coincidence peak [18,39] is a result of broadening of the emission line (see Fig. 4 and the definition of the correlation functions in the Appendix). The HOM interference visibility is determined by comparing parallel- and cross-polarized coincidence peak areas $V = 1 - G_{3,4}^{(2)}(0)_{\parallel} / G_{3,4}^{(2)}(0)_{\perp} = 0.53 \pm 0.03$ and amounts

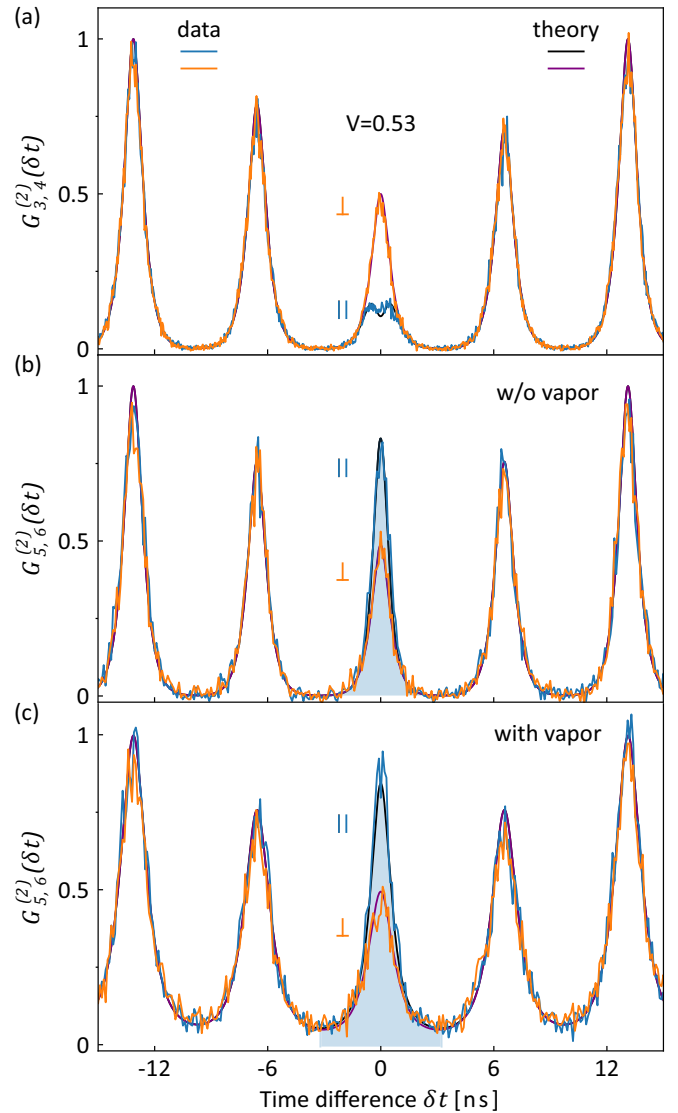


FIG. 2. Correlation measurements. (a) Hong-Ou-Mandel (HOM) interference detected at the two output ports of BS_1 of the HOM interferometer [see Fig. 1(a)]. Parallel polarized interfering photons (\parallel , blue) are compared to noninterfering perpendicular polarized photons (\perp , orange), which yields the visibility of $V = 0.53$. Theory curves are plotted behind the data. (b) Correlation measurement at the output ports of BS_2 following one HOM interferometer output port. In this constellation, interfering photons at BS_1 are signified by increased coincidences at BS_2 , which yields again the same visibility. The events contained in the shadowed coincidence peak are postselected for the data in Fig. 3. (c) Same correlation measurement as in (b), but with the Cs vapor in the propagation path of the photons.

to the fidelity of the two-photon state, which is generated upon HOM interference, to the two-photon Fock state.

The observed coalescence should imply both preparation of the desired two-photon NOON state and consequently, bunching of photons in one output port. To investigate this, we link one output arm of the HOM setup to BS_2 for a correlation measurement at ports 5 and 6. The projection of

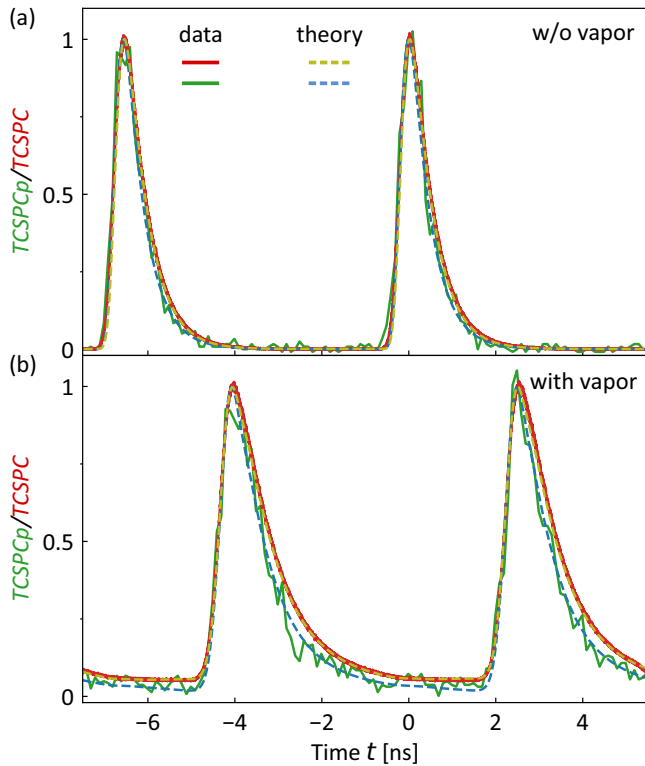


FIG. 3. Delayed Fock states. (a) Time-correlated single-photon counting (TCSPC) for the one-photon Fock state $|1\rangle$ (red curve, 1 ps binning, all detection events) and the two-photon Fock state $|2\rangle$ [green line, 100 ps binning, postselected on events within the highlighted coincidence peak in Figs. 2(b) and 2(c)] detected at port 6 (TCSPCp), without vapor. The dashed yellow curve is an exponential fit (decay constant $\tau = 0.43$ ns) under consideration of the APD response. The dashed blue curve is a simulation for two-photon states. (b) TCSPC with the propagation of photons through the Cs vapor. Color code as in (a).

only one output path leaves a two-photon Fock state $|2\rangle$, which is inspected in the central coincidence peak of the correlation histogram [Fig. 2(b)]. Considering the cross-polarized case, we find again the same pattern as before at the outputs of the HOM setup. However, for the parallel case, the central coincidence peak displays a strong increase as opposed to the coalescence previously observed. This demonstrates the successful generation of $|2\rangle$ states at BS_1 and their consequent propagation and detection. The reduced coincidences present in the HOM measurement have increased, as expected (see Fig. 4), the probability of finding pairs of photons in one output arm (here three). Notably, the analysis of the peak areas fully reproduces the visibility of the HOM measurements. The value is again $V = |1 - G_{5,6}^{(2)}(0)_{\parallel}/G_{5,6}^{(2)}(0)_{\perp}| = 0.53 \pm 0.04$.

In the next step, the same experimental configuration is used to propagate the two-photon state through the Cs vapor and to investigate its transmission and whether it can survive the interaction with a slow-light medium. For that, the hot Cs vapor is included into the path of the photons. The correlation histogram acquired after the propagation through the vapor at ports 5 and 6 is depicted in Fig. 2(c). It shows the same qualitative peak pattern with the same visibility as before,

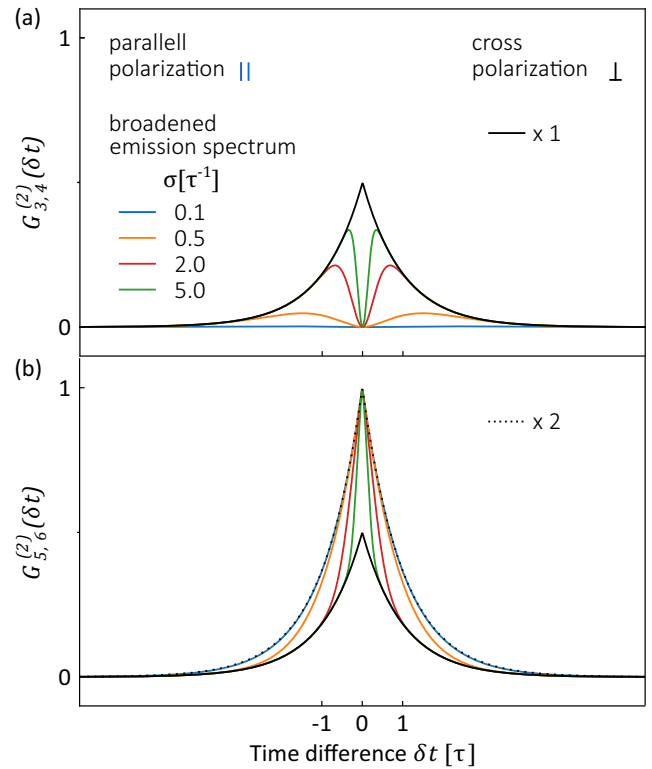


FIG. 4. Theory: (a) HOM interference at BS_1 in the presence of line broadening of the emission with standard deviation σ of broadened spectrum as specified in Eq. (A7). The black curve represents the noninterfering case of cross-polarized photons. (b) Photon correlation at BS_2 for the same cases as considered in (a). The dashed black curve shows twice the cross-polarized curve for comparison. The coincidences reduced in (a) are cumulated in the coincidence of (b). In the actual experiment, detector jitter prohibits the narrow dip from reaching zero and the narrow peak from reaching 1.

proving the preserved fidelity of the two-photon state and successful propagation of the $|2\rangle$ state through the slow-light medium. This feature of the two-photon state complements properties of the one-photon Fock state upon the interaction with a vapor, which previously was shown to preserve photon statistics and photonic coherence [24] in that case.

Note that the peaks in the histogram display broadening as a result of pulse distortion that is closely connected to the vapor response and the presence of QD spectral diffusion [24,34]. It is worth mentioning that the effect of detector jitter is reduced due to this temporal broadening. In particular, the temporal shape of the central coincidence peak, which signifies the generated $|2\rangle$ state, remains narrower than all other peaks of correlations from temporally separate single photons, as expected for nonunity two-photon interference, and the coincidence peak reaches closer to the theoretical maximum when the vapor is in the photons path. Simulation curves which include the vapor response and the results gained in the HOM measurements without the vapor excellently fit the data underpinning the preservation of the two-photon state after the vapor.

B. Temporal delay of Fock states

Having shown the successful generation of photon pairs in the $|2\rangle$ state outlasting the interaction with the vapor, we now investigate the vapor-induced delay by means of TCSPC for the two Fock states $|1\rangle$ and $|2\rangle$.

Figure 3(a) shows TCSPC detected at port 6 of BS₂ for the case of parallel-polarized photons. Postselection of a coincidence event within the highlighted bunching peaks of Fig. 2(b) delivers TCSPCp for the $|2\rangle$ state. Taking all other detection events yields TCSPC for the $|1\rangle$ state. We find the detection times and the temporal shapes of both photon states to be similar. As for the $|2\rangle$ state, a slightly narrower temporal shape is anticipated as is the case for the central coincidence peak. However, both the severe limitation of detection rates due to the postselection which results in a higher statistical deviation in each bin and the detector jitter prevent a clear distinction of the temporal shapes of the quantum states.

Figure 3(b) shows the TCSPC and TCSPCp measurements after the propagation of parallel-polarized photons through the Cs vapor using the same detection procedure as before. The arrival time of photons is now delayed by ~ 3 ns due to decreased group velocity in the atomic vapor for the photons of both Fock states. This delay already enables applications such as slow-light Fourier transform interferometry [35] or tuning in and out of synchronization of photonic signals. Moreover, the accordance of delays for both Fock states implies that the achieved fractional delay of 50 for one-photon Fock states [24] lies also within the potential of two-photon states.

Note that both Fock states display a temporal broadening due to chromatic dispersion of the vapor [24,34]. This broadening turns out to be beneficial for distinguishing the temporal shapes of the states. Due to emission line broadening the two-photon interference yields a narrower temporal form in TCSPC than it does in the correlation measurements. Simulations (dashed curves) that take the known spectral diffusion process for this QD [34] into account, reproduce the data faithfully. It is worth mentioning that for a Fourier-limited emitter, the temporal shapes of a one-photon Fock state and a pure two-photon Fock state do not differ. In this respect, the photon statistics via a correlation measurement at a beam splitter is a mandatory tool to distinguish between the Fock states.

III. DISCUSSION

In summary, we utilized the bunching of indistinguishable single photons at a beam splitter, as a result of the HOM interference, to generate a two-photon Fock state. We verified the accordance of coalescence in the HOM measurement with the bunching of photons in one of the output ports via a correlation measurement on the two-photon state, where both measurements showed the same visibility. The interaction of the two-photon state with a dispersive cesium vapor compares to the single-photon case as signified by the same acquired delay. While the emission line broadening induces a slight narrowing of the temporal form of the two-photon state, the correlation measurements after the vapor show unchanged visibility and thereby proves the preservation of the two-photon state. Thus, we experimentally verified that higher number Fock states ($N = 2$) show no hindrance to be

utilized in slow-light media. This combination can open new perspectives in interferometry, reinforcing the enhancement in spectral phase sensitivity provided by the slow-light effect [35–37] with the enabling feature of the two-photon Fock state for phase measurements with superresolution and supersensitivity [6–8,12].

ACKNOWLEDGMENTS

We acknowledge financial support from the DFG (MI 500/31-1). S.L.P. gratefully acknowledges the BW Stiftung “Post-doc Eliteprogramm” via the project Hybrideye. We also acknowledge Swabian Instruments (Time Tagger) for technical support. We thank Robert Löw, Julian Maisch, and Jonas Weber for fruitful discussions.

APPENDIX

1. Propagation of a single photon in a linear dispersive medium

A single-photon Fock state with wave packet χ can be described [45] as $|1\rangle = \int d\omega \chi(\omega) \hat{a}^\dagger(\omega) |0\rangle$. Here $\hat{a}^\dagger(\omega)$ is a bosonic creation operator at a single angular frequency ω . Via Fourier transformation \mathcal{FT} the temporal wave packet is obtained:

$$\chi(t) = \mathcal{FT}\{\chi(\omega)\} = \int \frac{d\omega}{\sqrt{2\pi}} e^{-i\omega t} \chi(\omega). \quad (\text{A1})$$

The propagation of a photon pulse in a dispersive medium leads to a frequency-dependent phase change which is described by the transformation

$$\hat{a}(\omega) \mapsto e^{-i\omega L n(\omega)/c} \hat{a}(\omega), \quad (\text{A2})$$

where L is the propagation distance, c the speed of light, and $n(\omega)$ is the index of refraction. Note that the complex refractive index $n(\omega) \mapsto n(\omega) + \frac{i}{2\omega/c} \alpha(\omega)$ will be used to account for the absorption according to Beer-Lambert’s law, induced by the coefficient $\alpha(\omega)$.

The general amplitude spectrum of a Lorentzian photon generated as a result of spontaneous emission after π -pulse excitation takes the following form after propagation along L in the vapor (indicated by the superscript):

$$\chi_0^L(\omega) = \sqrt{\frac{2\tau}{\pi}} \frac{e^{i\omega t_0}}{1 - 2i\tau(\omega - \omega_0)} e^{i\omega L n(\omega)/c}, \quad (\text{A3})$$

where t_0 is the time of photon generation, τ the decay constant, and ω_0 the carrier frequency of the wave packet, which will be indicated by the subscript.

2. Photon correlation

The Hong-Ou-Mandel interference [25,26] is usually studied by photon-correlation measurements at different outputs $G_{3,4}^{(2)}(\delta t)$ where reduced coincidences signify successful interference. Alternatively, correlations in one output arm $G_{3,3}^{(2)}(\delta t)$ can be used, where successful interference is signified by increased coincidences [23,40]. The correlation histograms can be described in a time-resolved manner following Ref. [39]. Two parallelly polarized single photons $|\Psi\rangle = |1\chi_1^0\rangle_1 \otimes |1\chi_2^0\rangle_2$ entering BS₁ simultaneously from the

different spatial modes, which are indicated by the subscript of the kets, yield the correlations

$$G_{3,4}^{(2)}(\delta t) \propto \int dt \frac{1}{4} |\chi_1^0(t + \delta t)\chi_2^0(t) - \chi_1^0(t)\chi_2^0(t + \delta t)|^2, \quad (\text{A4})$$

$$G_{3,3}^{(2)}(\delta t) \propto \int dt \frac{1}{4} |\chi_1^0(t + \delta t)\chi_2^0(t) + \chi_1^0(t)\chi_2^0(t + \delta t)|^2, \quad (\text{A5})$$

where $G_{i,j}^{(2)}(\delta t) = \int dt \langle \Psi | \hat{a}_i(t) \hat{a}_j(t + \delta t) \hat{a}_j^\dagger(t + \delta t) \hat{a}_i^\dagger(t) | \Psi \rangle$.

If the photons are in orthogonal polarizations H and V the correlations display intensities only and no interference occurs as expected:

$$G_{i,j}^{(2)}(\delta t) \propto \int dt \frac{1}{4} (|\chi_1^0(t + \delta t)\chi_2^0(t)|^2 + |\chi_1^0(t)\chi_2^0(t + \delta t)|^2). \quad (\text{A6})$$

The Gaussian broadened emission spectrum can be included into the description by integrating over a normal distribution $\mathcal{N}(\mu, \sigma^2)$ with variance σ^2 [18,39] and mean μ . The full width at half maximum (FWHM) of the emission line is given through $\text{FWHM} = 2\sqrt{2 \ln(2)}\sigma$. In the presence of this inhomogeneous broadening, the central peak of the histograms is obtained as

$$\langle G_{i,j}^{(2)}(\delta t) \rangle_{\mathcal{N}(0, 2\sigma^2)} = \frac{1}{4\tau} e^{-|\delta t|/\tau} (1 \mp e^{-\sigma^2 \delta t^2}), \quad (\text{A7})$$

where $\langle G_{i,j}^{(2)}(\delta t) \rangle_f = \int d(\delta\omega) f(\delta\omega) G_{i,j}^{(2)}(\delta t)$ integrates over the carrier frequency differences of the photons $\delta\omega$, while the minus (plus) in the brackets is to be taken for the correlations of different (same) output modes.

Despite broadening of the emission spectrum, coincidences at different outputs still completely vanish for $\delta t = 0$. This is shown for various emission linewidths in Fig. 4(a). Note that in Eq. (A7), the coincidences that are reduced in the correlations at different outputs are added for the correlations within one output mode. Figure 4(b) shows the corresponding coincidences in one output arm for the various linewidths. For broader emission linewidths, the dip at opposite outputs or the peak in one output arm gets narrower; however, reaching always the theoretical minimum of zero or maximum of one, respectively. In the experiments, we used an additional beam splitter to measure the correlation which is present in one output arm of the HOM setup (port 3). This allows one to acquire the targeted histogram since the correlations at ports (5 and 6) at the BS₂ reproduce the same histogram, i.e., $G_{3,3}^{(2)}(\delta t) \propto G_{5,6}^{(2)}(\delta t)$, with coincidence rate being the only compromise. In the experiment, detector jitter prevents the resolution of the aforementioned features, while the modulation of the central peaks still indicate the effect.

To properly describe the experimental data with the vapor in the path of the photons, relations (A2) and (A3) were exploited. Moreover, the theory curves on top of the data take into account the known spectral diffusion parameters from a previous study on the same QD [34].

3. Postselected TCSPC

TCSPC is calculated via $\langle \Psi | \hat{a}_6(t) \hat{a}_6^\dagger(t) | \Psi \rangle$ with $|\Psi\rangle = |1\chi_1^L\rangle_6$ or $|\Psi\rangle = \frac{1}{\sqrt{2}}(|1\chi_1^L\rangle_5 \otimes |1\chi_2^L\rangle_6 + |1\chi_2^L\rangle_5 \otimes |1\chi_1^L\rangle_6)$ for one- or two-photon states postselected on a coincidence (TC-SPCp), respectively. The simulation curves on top of the data additionally take the known spectral diffusion processes into account.

-
- [1] *Quantum Dots for Quantum Information Technologies*, edited by P. Michler (Springer International Publishing, New York, 2017).
- [2] Y.-M. He, Y. He, Y.-J. Wei, D. Wu, M. Atatüre, C. Schneider, S. Höfling, M. Kamp, C.-Y. Lu, and J.-W. Pan, *Nat. Nanotechnol.* **8**, 213 (2013).
- [3] M. Müller, S. Bounouar, K. D. Jöns, M. Glässl, and P. Michler, *Nat. Photonics* **8**, 224 (2014).
- [4] J. Liu, R. Su, Y. Wei, B. Yao, S. F. C. da Silva, Y. Yu, J. Iles-Smith, K. Srinivasan, A. Rastelli, J. Li, and X. Wang, *Nat. Nanotechnol.* **14**, 586 (2019).
- [5] H. Wang, J. Qin, X. Ding, M.-C. Chen, S. Chen, X. You, Y.-M. He, X. Jiang, L. You, Z. Wang, C. Schneider, J. J. Renema, S. Höfling, C.-Y. Lu, and J.-W. Pan, *Phys. Rev. Lett.* **123**, 250503 (2019).
- [6] T. Nagata, R. Okamoto, J. L. O'Brien, K. Sasaki, and S. Takeuchi, *Science* **316**, 726 (2007).
- [7] M. W. Mitchell, J. S. Lundeen, and A. M. Steinberg, *Nature (London)* **429**, 161 (2004).
- [8] M. Müller, H. Vural, C. Schneider, A. Rastelli, O. G. Schmidt, S. Höfling, and P. Michler, *Phys. Rev. Lett.* **118**, 257402 (2017).
- [9] T. Jennewein, C. Simon, G. Weihs, H. Weinfurter, and A. Zeilinger, *Phys. Rev. Lett.* **84**, 4729 (2000).
- [10] C. Simon, H. de Riedmatten, M. Afzelius, N. Sangouard, H. Zbinden, and N. Gisin, *Phys. Rev. Lett.* **98**, 190503 (2007).
- [11] L. Upton, M. Harpham, O. Suzer, M. Richter, S. Mukamel, and T. Goodson, *J. Phys. Chem. Lett.* **4**, 2046 (2013).
- [12] A. J. Bennett, J. P. Lee, D. J. P. Ellis, T. Meany, E. Murray, F. F. Floether, J. P. Griffiths, I. Farrer, D. A. Ritchie, and A. J. Shields, *Sci. Adv.* **2**, e1501256 (2016).
- [13] E. del Valle, A. Gonzalez-Tudela, E. Cancellieri, F. P. Laussy, and C. Tejedor, *New J. Phys.* **13**, 113014 (2011).
- [14] S. Schumacher, J. Förstner, A. Zrenner, M. Florian, C. Gies, P. Gartner, and F. Jahnke, *Opt. Express* **20**, 5335 (2012).
- [15] C. S. Muñoz, E. del Valle, A. G. Tudela, K. Müller, S. Lichtmannecker, M. Kaniber, C. Tejedor, J. J. Finley, and F. P. Laussy, *Nat. Photonics* **8**, 550 (2014).
- [16] J.-H. Kim, S. Aghaieimibodi, C. J. K. Richardson, R. P. Leavitt, and E. Waks, *Nano Lett.* **18**, 4734 (2018).
- [17] J. H. Weber, J. Kettler, H. Vural, M. Müller, J. Maisch, M. Jetter, S. L. Portalupi, and P. Michler, *Phys. Rev. B* **97**, 195414 (2018).
- [18] J. H. Weber, B. Kambs, J. Kettler, S. Kern, J. Maisch, H. Vural, M. Jetter, S. L. Portalupi, C. Becher, and P. Michler, *Nat. Nanotechnol.* **14**, 23 (2019).

- [19] H. Vural, S. L. Portalupi, and P. Michler, *Appl. Phys. Lett.* **117**, 030501 (2020).
- [20] K. A. Fischer, L. Hanschke, J. Wierzbowski, T. Simmet, C. Dory, J. J. Finley, J. Vučković, and K. Müller, *Nat. Phys.* **13**, 649 (2017).
- [21] J. C. Loredó, C. Antón, B. Reznichenko, P. Hilaire, A. Harouri, C. Millet, H. Ollivier, N. Somaschi, L. De Santis, A. Lemaître, I. Sagnes, L. Lanco, A. Auffèves, O. Krebs, and P. Senellart, *Nat. Photonics* **13**, 803 (2019).
- [22] M. Bouillard, G. Boucher, J. Ferrer Ortas, B. Pointard, and R. Tualle-Brouri, *Phys. Rev. Lett.* **122**, 210501 (2019).
- [23] W. Zhang, M.-X. Dong, D.-S. Ding, S. Shi, K. Wang, Z.-Y. Zhou, G.-C. Guo, and B.-S. Shi, *Phys. Rev. A* **98**, 063820 (2018).
- [24] H. Vural, S. L. Portalupi, J. Maisch, S. Kern, J. H. Weber, M. Jetter, J. Wrachtrup, R. Löw, I. Gerhardt, and P. Michler, *Optica* **5**, 367 (2018).
- [25] C. K. Hong, Z. Y. Ou, and L. Mandel, *Phys. Rev. Lett.* **59**, 2044 (1987).
- [26] C. Santori, D. Fattal, J. Vučković, G. S. Solomon, and Y. Yamamoto, *Nature (London)* **419**, 594 (2002).
- [27] M. A. Zentile, J. Keaveney, L. Weller, D. J. Whiting, C. S. Adams, and I. G. Hughes, *Comput. Phys. Commun.* **189**, 162 (2015).
- [28] R. M. Camacho, M. V. Pack, J. C. Howell, A. Schweinsberg, and R. W. Boyd, *Phys. Rev. Lett.* **98**, 153601 (2007).
- [29] N. Akopian, L. Wang, A. Rastelli, O. G. Schmidt, and V. Zwiller, *Nat. Photonics* **5**, 230 (2011).
- [30] R. Trotta, J. Martín-Sánchez, J. S. Wildmann, G. Piredda, M. Reindl, C. Schimpf, E. Zallo, S. Stroj, J. Edlinger, and A. Rastelli, *Nat. Commun.* **7**, 10375 (2016).
- [31] T. Kroh, J. Wolters, A. Ahlrichs, A. W. Schell, A. Thoma, S. Reitzenstein, J. S. Wildmann, E. Zallo, R. Trotta, A. Rastelli, O. G. Schmidt, and O. Benson, *Sci. Rep.* **9**, 13728 (2019).
- [32] J. Maisch, H. Vural, M. Jetter, P. Michler, I. Gerhardt, and S. L. Portalupi, *Adv. Quantum Technol.* **3**, 1900057 (2020).
- [33] S. L. Portalupi, M. Widmann, C. Nawrath, M. Jetter, P. Michler, J. Wrachtrup, and I. Gerhardt, *Nat. Commun.* **7**, 13632 (2016).
- [34] H. Vural, J. Maisch, I. Gerhardt, M. Jetter, S. L. Portalupi, and P. Michler, *Phys. Rev. B* **101**, 161401(R) (2020).
- [35] Z. Shi, R. W. Boyd, R. M. Camacho, P. K. Vudya Setu, and J. C. Howell, *Phys. Rev. Lett.* **99**, 240801 (2007).
- [36] Z. Shi and R. W. Boyd, *J. Opt. Soc. Am. B* **25**, C136 (2008).
- [37] U. Bortolozzo, S. Residori, and J. C. Howell, *Opt. Lett.* **38**, 3107 (2013).
- [38] K. D. Jöns, R. Hafenbrak, R. Singh, F. Ding, J. D. Plumhof, A. Rastelli, O. G. Schmidt, G. Bester, and P. Michler, *Phys. Rev. Lett.* **107**, 217402 (2011).
- [39] T. Legero, T. Wilk, A. Kuhn, and G. Rempe, *Characterization of Single Photons using Two-Photon Interference*, Advances in Atomic, Molecular, and Optical Physics Vol. 53, edited by G. Rempe and M. Scully (Elsevier, Amsterdam, 2006), pp. 253–289.
- [40] M. Rezai, J. Wrachtrup, and I. Gerhardt, *Phys. Rev. X* **8**, 031026 (2018).
- [41] A. V. Kuhlmann, J. Houel, A. Ludwig, L. Greuter, D. Reuter, A. D. Wieck, M. Poggio, and R. J. Warburton, *Nat. Phys.* **9**, 570 (2013).
- [42] M. J. Stanley, C. Matthiesen, J. Hansom, C. Le Gall, C. H. H. Schulte, E. Clarke, and M. Atatüre, *Phys. Rev. B* **90**, 195305 (2014).
- [43] C. Schimpf, M. Reindl, P. Klenovský, T. Fromherz, S. F. C. D. Silva, J. Hofer, C. Schneider, S. Höfling, R. Trotta, and A. Rastelli, *Opt. Express* **27**, 35290 (2019).
- [44] P. Michler, A. Kiraz, C. Becher, W. V. Schoenfeld, P. M. Petroff, L. Zhang, E. Hu, and A. Imamoğlu, *Science* **290**, 2282 (2000).
- [45] R. Loudon, *The Quantum Theory of Light* (Oxford University Press, Oxford, 2000).